HHS Public Access

Author manuscript

FASEB J. Author manuscript; available in PMC 2021 September 01.

Published in final edited form as:

FASEB J. 2020 September ; 34(9): 12549–12564. doi:10.1096/fj.202000851R.

Antibody Screening Using a Human iPSC-based Blood-Brain Barrier Model Identifies Antibodies that Accumulate in the CNS

Julia V. Georgieva[1,2], **Loukas I. Goulatis**[1,2], **Charles C. Stutz**[2], **Scott G. Canfield**[2,4], **Hannah W. Song**[2], **Benjamin D. Gastfriend**[2], **Eric V. Shusta**[*,2,3]

[2]Department of Chemical and Biological Engineering, University of Wisconsin-Madison, Madison, Wisconsin, USA

[3]Department of Neurological Surgery University of Wisconsin-Madison, Madison, Wisconsin, USA

[4]Current Affiliation: Department of Cellular and Integrative Physiology, Indiana University School of Medicine, Terre Haute, IN, 47809

Abstract

Drug delivery across the blood-brain barrier (BBB) remains a significant obstacle for the development of neurological disease therapies. The low penetration of blood-borne therapeutics into the brain can oftentimes be attributed to the restrictive nature of the brain microvascular endothelial cells (BMECs) that comprise the BBB. One strategy beginning to be successfully leveraged is the use of endogenous receptor-mediated transcytosis (RMT) systems as a means to shuttle a targeted therapeutic into the brain. Limitations of known RMT targets and their cognate targeting reagents include brain specificity, brain uptake levels and off-target effects, driving the search for new and potentially improved brain targeting reagent-RMT pairs. To this end, we deployed human induced pluripotent stem cell (iPSC)-derived BMEC-like cells as a model BBB substrate on which to mine for new RMT-targeting antibody pairs. A nonimmune, human single-chain variable fragment (scFv) phage display library was screened for binding, internalization and transcytosis across iPSC-derived BMECs. Lead candidates exhibited binding and internalization into BMECs as well as binding to both human and mouse BBB in brain tissue sections. Antibodies targeted the murine BBB after intravenous administration with one particular clone, 46.1-scFv, exhibiting a 26-fold increase in brain accumulation (8.1 nM). Moreover, clone 46.1-scFv was found to associate with postvascular, parenchymal cells, indicating its successful receptor-mediated transport across the BBB. Such a new BBB targeting ligand could enhance the transport of therapeutic molecules into the brain.

[*]Correspondence: Eric V. Shusta, Department of Chemical and Biological Engineering, Department of Neurological Surgery, University of Wisconsin-Madison, 1415 Engineering Drive, Madison, WI 53706, eshusta@wisc.edu, Ph: (608) 265-5103, Fax: (608) 262-5434.

Author contributions:

J.V. Georgieva., L.I. Goulatis., C.C. Stutz, S.G. Canfield, H.W. Song and B.D.Gastfriend performed the experiments. J.V. Georgieva, L.I. Goulatis and E.V. Shusta designed the experiments, analyzed the results and wrote the paper.

[1]These authors contributed equally.

Competing interests:

J.V.G., L.I.G. C.C.S and E.V.S. are inventors on a provisional US patent application.

Introduction:

The blood-brain barrier (BBB) prevents substantial accumulation of biologics in the central nervous system (CNS) after systemic administration, thereby limiting new treatments for neurological disorders. In the brain, the blood vessel network is made up of brain microvascular endothelial cells (BMECs) connected by tight junctions that restrict paracellular movement of molecules into the CNS, hence, controlling brain uptake of blood-borne substances (1). For instance, brain uptake of untargeted antibodies is limited to ~0.1% of circulating antibody levels (2), hampering therapeutic effects from a systemically administered biologic. However, a host of molecular transporters are expressed by BMECs that allow the selective passage of necessary nutrients across the BMECs by carrier-mediated and receptor-mediated transport (RMT) mechanisms. Thus, one approach to circumvent barrier properties consists of coopting BBB RMT systems by targeting them with antibodies that can first engage the RMT receptor on the blood side of BMECs and trigger transcytosis of the targeting antibody and any attached therapeutic cargo across the BMECs and into the brain (3). Two prominent examples are antibodies against the transferrin (TfR) (4) and insulin (IR) receptors (5). These systems, while mediating transport across the BBB, are somewhat inefficient and non-specific, and can result in deleterious off-target effects (6–8).

While it is possible to mitigate these effects by antibody engineering strategies (9), there remains a significant need for the discovery of new BBB RMT-targeting antibody pairs that may address these challenges. Several approaches have been implemented to identify new antibody-RMT pairs (10). Genomic and proteomic profiling of BBB endothelial cells has helped identify new BBB RMT targets such as basigin and CD98 heavy chain (11); however, it can be difficult to determine a priori what BBB proteins identified from omics data are actually capable of BBB transport. By contrast, phenotypic screening of large antibody libraries on a variety of BBB substrates can be used to identify cognate antibody-RMT pairs without prior knowledge of the RMT target (10). However, unlike genomic and proteomic approaches in which the BBB target receptor is known, phenotypic screening requires downstream target receptor identification (12). To date, phenotypic screening of large libraries in vivo (13, 14) and in vitro (15, 16) for new antibody-RMT pairs has shown limited success, with only a handful of new BBB targeting antibodies isolated. In vivo screening challenges include the finding that phage antibody libraries are plagued by high background recoveries masking relevant clones (16), while antibodies identified from in vitro biopanning often do no not cross-react with in vivo antigens, due to potential alteration of protein expression profiles in culture. Further, human in vitro BBB models based on primary or immortalized BMECs are inherently leaky, limiting the effectiveness of functional transcytosis screens of antibody libraries. To address these issues, we employed a new screening paradigm relying on human induced pluripotent stem cell (iPSC)-derived BMEC-like cells (iPSC-derived BMECs) as a screening substrate. The iPSC-derived BMECs, have well-developed tight junctions, express key BBB markers and, most importantly for the application described here, are a reasonable facsimile of both primary human BMECs and acutely isolated human BMECs in terms of their transporter expression profiles (17–20). While several iPSC-derived BBB models with sufficient barrier function

are available (21–25), they have not been employed for identification of new BBB penetrating antibodies. Thus, we used iPSC-derived BMECs to perform a transcytosis screen with a phage display scFv library and identified a cohort of antibodies able to react with human BBB antigens and target the murine brain vasculature in vivo. Two lead antibodies investigated in more detail demonstrated increased brain accumulation and were found associated with post vascular cells, suggesting their potential utility for CNS therapeutic delivery.

Materials and Methods:

Cell culture:

BMEC differentiation was performed as previously described using the IMR90-C4 iPSC line and retinoic acid induction (18, 19). At day 8 of differentiation, BMECs were plated on collagen/fibronectin coated tissue culture plates or 1 μm pore size poly-ester transwells (Corning #CLS3462). The primary human lung and heart microvascular endothelial cells (hLECs and hCECs, CC-2527 and CC-7030) were obtained from LONZA (Walkersville, MD), and cultured as per manufacturer's instructions.

Phage screen:

All the screening methods are adapted from protocols outlined in Zhou and Marks using the previously described fd-tet based human scFv library (26–28). Initially, the human scFv library was pre-subtracted by serial application on hLECs and hCECs grown on T-75 flasks. All screening rounds were performed in appropriate culture media for each cell type. In each round 10^{11} colony forming units (CFU) were applied to a confluent cell monolayer. Pre-subtraction rounds were performed by incubating the library on monolayers for 1 hr on ice, while internalization rounds on BMECs were performed by incubating the phage library on BMECs for 1 hr at 37 °C. Following phage internalization, media was aspirated and cells were washed 1X with stripping buffer I (150mM NaCl, 100mM Glycine, pH 2.5) and 2X with stripping buffer II (500mM NaCl, 50mM Glycine, 0.2M Urea, pH 2.8) for 5 min at RT to remove membrane bound phage. BMECs were detached by trypsin treatment and spun down at 300g at 4°C for 5 min. The cell pellet was then resuspended in ice-cold lysis buffer (triethanolamine 100mM), incubated on ice for 15 min, and neutralized (Tris-HCl pH 7.4). Phage eluted from each selection round were then used to infect log phase E. coli TG1 cells. Phage particles were rescued from the bacteria, amplified and used for subsequent rounds of antibody screening as previously described (29). A total of 1 pre-subtraction and 3 internalization rounds were performed.

For transcytosis screens, 10^{11} CFU from the third internalization round was dosed on top of a BMECs monolayer on a 1 μm pore size transwells with a minimum TEER of 1000 ohm-cm^2 and allowed to transcytose for 3 hrs at 37 °C before harvesting phage containing media from the bottom chamber for TG1 infection. For the competition transcytosis screen selection, 10^{11} CFU from the third internalization round were dosed onto BMECs along with 1 μM of soluble scFv 3 and 22Ch and allowed to transcytose for 3 hrs at 37 °C before harvesting phage containing media from the bottom chamber for TG1 infection.

Individual phage-infected TG1 colonies were grown overnight, and DNA was heat-extracted and PCR amplified using primers that flank the scFv gene. The primer sequences were 5′-TTTTTGGAGATTTTCAACGTGA-3′, and 5′-GAATTTTCTGTATGAGGTTTTGCTAAA-3′ for the forward and reverse primers, respectively. PCR fragments were then Sanger sequenced (UW Madison Biotechnology Center Sequencing facility).

Phage immunocytochemistry:

BMECs were purified on 96-well tissue culture plates as described above. The day of the assay, each well of BMECs was blocked with 250 μL of PBS with calcium and magnesium (PBSCM; PBS with 1 mM of calcium chloride and 0.5 mM of magnesium sulfate) supplemented with 40% goat serum (PBSCMG) (Sigma–Aldrich, #G6767). The wells were washed three times with 250 μl of PBSCM. Next, cells were fixed with paraformaldehyde (PFA, 4% w/v in PBS) for 10 min at RT. Overnight cultures of phage harboring bacteria were centrifuged, and 50 μl of the phage containing supernatant from each sample were incubated directly on the BMECs in the presence of 100 μl of fresh PBSCMG. The plate was incubated for 1 hr at 4°C and then washed once. An anti-M13 antibody (GE healthcare #27942001) diluted 1:500 in PBSCMG was incubated in each well for 1 hr at 4°C. Cells were washed with PBSCM, and incubated with secondary antibody, goat anti-mouse AlexaFluor488 for 30 min at 4°C. Next, the cells were washed three times in PBSCM and post-fixed for 8 min at RT with PFA. The plate was then imaged on an Olympus epifluorescence microscope (Center Valley, PA).

Soluble scFv and scFv-Fc preparation:

The following method for production of soluble scFv-His6 fusions is based on a protocol described in (29). An overnight bacterial culture transformed with the scFv secretion plasmid was used to inoculate 2xYT medium containing 100 μg/mL ampicillin and 0.1% glucose, which was then grown at 37°C until an $OD_{600\ nm}$ of 0.9 was reached. Expression was induced by addition of 1 mM isopropyl-β-D-thiogalactopyranoside (IPTG, Fisher Scientific, # 50213380) and bacteria allowed to grow for 4 hrs at 30°C. The bacteria was harvested and the scFv recovered by serial incubation with a periplasmic extraction buffer (PPB, 200 g/L sucrose, 1 mM EDTA, 30 mM tris–HCl, pH 8.0) supplemented with DNAse I (Roche Applied Sciences, # 10104159001) to 100 μg/ml, and complete Mini protease inhibitor cocktail tablets (Roche Applied Sciences, # 11836153001) followed by an osmotic shock buffer (OSB, 5 mM magnesium sulfate in ddH2O) supplemented with DNAse I and complete Mini protease inhibitor cocktail. The resulting solution was syringe filter sterilized, and dialyzed against PBS + 10 mM imidazole. The scFv were purified from the crude extract with Qiagen Ni-Nta Spin Columns (Qiagen #31014) using manufacturer recommended protocol for purification. The purified scFvs were eluted and subsequently dialyzed against PBS, and the purity of the scFv was verified by sodium dodecyl sulfate–polyacrylamide gel electrophoresis (SDS–PAGE) and Coomassie blue staining. Soluble scFvs were pre-dimerized with rabbit polyclonal anti *c-myc* antibody (Thermo fisher #PA1–981) in 4:1 molar ratio for 2 hrs in PBSG (10 % goat serum in PBS) and used as dimers for all downstream assays.

For scFv-Fc fusion production, scFv genes were fused to rabbit Fc region by subcloning into a pIRES-rabbit Fc vector (30) using NheI and AgeI restriction sites via standard PCR amplification, restriction digestion, and ligation procedures. As a negative control, a fusion of the same rabbit Fc to a variable lymphocyte receptor that binds to human H antigen trisaccharide was used (30, 31) (negative control, Ctrl-Fc). Large scale DNA purification for HEK 293F transfection was done with ZymoPURE II plasmid kit (Zymo Research # D4200), and 293fectin (ThermoFisher #12347019) transfection reagent was used. Transfected cultures were then incubated for 5 days at 37 °C, 8% CO_2, 135 rpm in a humidified incubator and the supernatant containing scFv-Fcs was separated from the cell mass via centrifugation and filtration. ScFv-Fcs were purified from the cleared supernatant via protein A/G chromatography (ThermoFisher #20423). After elution with 100 mM Citric Acid pH 3, the solution was neutralized with 1M Tris-base pH 9 and concentrated with protein concentrator (ThermoFisher #88502) before 4°C storage. Total protein concentration was quantified using UV 280 absorbance and extinction coefficients generated by ExPASy (http://web.expasy.org/protparam/).

Cell based assays:

Membrane binding and endocytosis assay: BMECs were purified on Lab Tek II chamber slides (Nunc #154917). Cells were washed once with PBS and incubated with blocking buffer PBSG (10 % goat serum in PBS) for 30 min on ice. Pre-dimerized scFvs (13.2 μg/ml) or scFv-Fcs (5 μg/ml) were added to BMECs and incubated for additional 30 min on ice to allow binding. The chamber slides were then transferred at 37°C for 30 min to allow internalization. Afterwards, cells were washed with cold PBS and incubated with anti-rabbit AlexaFluor555, 1:1000 in PBSG for 30 min on ice to label the membrane-bound fraction of scFv-Fcs. Cells were washed once more on ice, fixed with 4% PFA on ice for 10 min and permeabilized with 0.2% Triton X for 2 min. Anti-rabbit AlexaFluor488, 1:1000 in PBSG was used to label the internalized fraction for 30 min at RT. Finally, cells were washed and mounted with ProLong Gold antifade reagent with DAPI (Invitrogen, P36935). Images were acquired on Zeiss Axio Imager Z2 Upright microscope. For confocal microscopy experiments in Figure S2, BMECs were incubated with 5 μg/ml 46.1-scFv-Fc and incubated for various times at 37°C. The surface bound 46.1-scFv-Fc was visualized with anti-rabbit AlexaFluor647. After fixation and permeabilization, cells were additionally incubated with mouse anti-human ZO-1 (Invitrogen #339100) or mouse anti-human PECAM1/CD31 (Cell Sciences #MON6002–1), diluted 1:50 in PBSG for 45 min at RT, followed by secondary anti-mouse AlexaFluor488 and anti-rabbit AlexaFluor555, diluted 1:1000 in PBSG. Images were acquired on a Leica SP8 3X STED Confocal microscope.

Internalization assay: BMECs were purified on 96-well flat-bottomed plates (Corning #3539948). Cells were serum starved for 1 hr at 37° C in serum free endothelial medium. 1 μM purified scFv-Fc diluted in serum free medium were applied to cells. For temperature dependent internalization experiments, one group of samples was incubated at 37 °C and one group with the same concentration of scFv-Fc was incubated at 4°C for 1 hr. After scFv-Fc incubation, cell membrane-bound antibodies were stripped by 5X acid washing (100mM citric acid pH 3) on ice. Cells were fixed with 4% PFA for 8 min and blocked and permeabilized with 0.1% Triton X diluted in odyssey blocking buffer (LICOR #927–40000)

for 15 min. Internalized scFv-Fcs were detected by incubation for 1 hr at 4°C with IRdye800CW goat-anti-rabbit IgG pAb (LICOR #925–32211) and cell number in each well measured with CellTag (LICOR # 926–041090), both diluted in odyssey blocking buffer. After primary antibody incubation BMECs were washed on ice 7X with PBS 0.05 % Tween-20, and signal from each well measured with a LICOR Odyssey Imager with a focus offset of 3mm and resolution of 169μm. ScFv-Fc signal in each well was normalized to total cell number by dividing with the equivalent CellTag signal.

Equilibrium binding measurements: BMECs were purified on 96-well flat-bottomed plates, washed 2X with PBS, and fixed with 2% PFA for 8 min. Fixed cells were blocked and permeabilized as described above for LICOR imaging. Apparent equilibrium affinity titration measurements were performed by incubating fixed cells with a range of scFv-Fc concentrations ranging from 1 nM to 1 μM at RT for 2 hrs. After extensive washing with PBS 0.05 % Tween-20 at 4°C, cells were labeled for scFv-Fc detection and for total cell number evaluation with IRdye reagents and CellTag as described above. Fraction of cellular antigens bound by scFv-Fc was quantified using background subtracted, total cell number normalized binding signal and the data was fit to a bimolecular equilibrium binding model to determine the apparent dissociation constant (K_D).

Competition assay: scFv-Fcs were pre-incubated with $10XK_D$ concentrations of recombinant receptor ecto-domain proteins rIR (R&D Systems #1444-IR) and rhTfR (R&D Systems # 2474-TR) in PBS plus 1 % BSA for 30 min at room temperature and then applied to serum starved BMECs in 96 well plates to allow scFv-Fcs to bind to membrane antigens. Plates were incubated at 4°C for 2 hrs, and extensively washed, fixed and labeled with IRdye reagents for detection as described above. Total signal of the receptor-competed scFv-Fcs was compared to non-competed scFv-Fc signal intensity.

SDS-PAGE:

ScFv-Fcs were mixed with SDS containing sample buffer without reducing reagent and heated for 10 min prior to loading onto a 4–12 % Bis-Tris gel (ThermoFisher #NP0321). Gels were stained with Coomassie blue.

Flow cytometry:

BMECs were cultured in 6 wells plate as described above. The cells (~2×10^6 cells/sample) were washed in PBS and detached from the culture plate with versene treatment for 1 hr at 37 °C. The cells were transferred to 1.5 ml tubes and blocked for 1 hr at 4°C with PBS 1% BSA while rotating. 10^{11} CFU of phage (either from each round of panning, or negative control anti-botulinum toxin scFv displaying phage) were incubated with blocked BMECs for 1 hr at 4°C. Next, cells were washed 3X with PBS 1% BSA to remove weakly bound phage and labeled with anti-M13 antibody as described above. The cells were washed two times and resuspended in flow buffer (PBS + 0.1% BSA + 5 mM EDTA) and analyzed on a flow cytometer (Becton Dickinson FACSCalibur).

Immunolabeling of human and mouse brain cryosections:

Human brain tissue samples were obtained with approval from the University of Wisconsin-Madison Institutional Review Board and samples were snap frozen. Mouse brains were snap frozen in liquid nitrogen. Human and mouse tissue were cryosectioned in 8 and 30 μm sections on Thermo Scientific Microm HM 525. Due to the unknown structure of the corresponding antigens, multiple modes of fixation were used. Prior to immunolabeling, sections were fixed with either 4% PFA for 20 min at RT or in cold acetone at −20°C for 20 min. In some instances, sections were post-fixed after incubation with scFv-Fcs. Sections fixed with PFA were, additionally, permeabilized with 0.2% Tx-100 in PBS. Sections were blocked with 10% goat serum in PBS (PBSG) for 30 min at room temperature. ScFv-Fcs (5 μg/ml) were incubated on human and mouse brain sections for 24 hrs at 4°C. In human sections, the blood vessels were labeled with mouse anti-human PECAM1/CD31 (Cell Sciences #MON6002–1), diluted 1:50 in PBSG for 2 hrs at RT and secondary goat anti-mouse AlexaFluor488 (1:1000). The blood vessels in mouse brain sections were directly labeled with the lectin LEL DyLight488 (Vector laboratories LEL Dylight488). Tested antibodies were labeled with goat anti-rabbit AlexaFluor555 (1:1000) in PBSG. Sections were mounted with ProLong Gold antifade reagent with DAPI (Invitrogen, P36935), and mouse and human brains analyzed on Leica SP8 3X STED Confocal.

Immunolabeling of mouse brain cryosections after IV administration of antibodies:

Animal studies were approved by the Institutional Animal Care and Use Committee (IACUC) at the University of Wisconsin-Madison. Mice C57BL6, 5–6 weeks old, were injected intravenously via the retroorbital route with scFv-Fcs in a dose 5 mg/kg. Mice were subjected to whole-body perfusion at 5 ml/min for 5 min with a PBS, supplemented with 100 U/ml heparin, 4 μg/ml fluorescently labeled lectin (LEL Dylight488 Vector laboratories) and 0.1% BSA, followed by additional 5 min perfusion with 4% PFA in PBS. Brain, heart, lung, liver, kidney and spinal cord were collected and snap frozen in liquid nitrogen and stored at −80°C. Sections of 8 or 30 μm were made on Thermo Scientific Microm HM 525. Before immunolabeling, sections were air dried for 1 hr, permeabilized with 0.05% saponin for 30 min, and blocked with PBSG for 30 min at RT. To visualize bound scFv-Fcs, sections were incubated with anti-rabbit AlexaFluor555-conjugated secondary antibody (Invitrogen #A21428), diluted 1:1000 in PBSG with 0.05% saponin, overnight at 4°C. Washing steps were with 0.05% saponin in PBS. Sections were mounted with ProLong Gold antifade reagent with DAPI (Invitrogen, P36935) and analyzed on Zeiss Axio Imager Z2 Upright microscope. Additionally, 30 μm sections of injected mouse brain were immunolabeled for glial fibrillary acidic protein (GFAP) and collagen IV. After blocking with 10% goat or donkey serum, respectively and permeabilization as described previously, sections were incubated with either mouse anti-GFAP (BD Pharmingen #556329) or goat anti-collagen IV (Milipore Sigma #AB769) in the corresponding blocking buffer plus 0.05% saponin for 2 hrs at RT. Sections were washed with 0.05% saponin in PBS and incubated with secondary antibodies: anti-rabbit AlexaFluor555 (Invitrogen #A21428) and anti-mouse AlexaFluor647 (Invitrogen #A-21235) for GFAP detection or anti-rabbit AlexaFluor555 (Invitrogen #A31572) and anti-goat AlexaFluor647 (Invitrogen #A-21447) for collagen IV detection. Images were taken on Leica SP8 3X STED Confocal and processed with ImageJ. In some instances (Supplemental Fig. S6B) brain tissue was subjected to clearing with X-Clarity

technology (Logos Biosystems) as described in (32). Images for 3D reconstruction were acquired on Nikon A1R HD Upright Multi-Photon/Confocal microscope.

Quantification of antibodies in mouse brains with ELISA:

Mice C57BL6, 5–6 weeks old were injected intravenously with scFv-Fcs at a dose 20 mg/kg. After 1 hr, blood was sampled, briefly spun down and the plasma was frozen at −80°C until analysis. After whole body perfusion at a rate 5 ml/min for 10 min with a PBS, supplemented with 100 U/ml heparin and 0.1% BSA, brains were removed. To extract the accumulated antibody, brains were homogenized in 1% NP-40 in PBS with Complete Mini EDTA-free protease inhibitor cocktail tablets (Roche Diagnostics) as described previously (11). Next, brains were rotated at 4°C for 24 hrs. Supernatant was collected after centrifugation at 14,000 rpm for 20 min at 4°C. Brain extracts were either analyzed immediately or frozen at −80°C. No difference in the antibody brain concentration was observed in fresh or frozen samples.

Nunc Maxisorp 96-wells plates were coated with anti-HA tag antibody 1 μg/ml (Thermo Fisher Scientific #MA1–12429) diluted in 0.2 M $NaCO_3$/$NaHCO_3$. at 4°C overnight. Plates were washed three times 5 min each with 0,05% Tween-20 in PBS and blocked with 2% BSA in washing buffer. Brain extracts were added undiluted to the plate and blood plasma samples were diluted in blocking buffer. Antibodies with known concentration were diluted in NP-40 brain extracts prepared from untreated mice exactly as described above and added in serial dilutions to construct the standard curve for calculation of brain concentrations. The standard curve to determine the terminal plasma concentration was constructed from known concentration antibodies diluted in blocking buffer. After 2 hrs incubation at RT the samples were aspirated, the plate was washed three times 5 min each and anti-rabbit HRP antibody (Sigma #A6154) was added for 1 hr at RT. The unbound detection antibody was washed six times 5 min each and 1-Step Ultra TMB-ELISA Substrate Solution (ThermoFisher Scientific #34028) was added. Absorbance was measured at 450 nm on Infinite M200 (Tecan) plate reader. The lower limit of detection in brain samples was 1.03 nM, 0.02 nM and 0.44 nM for clone 46.1, 17 and Ctrl-Fc, respectively. The plasma concentration for clones 46.1 and Ctrl was determined with ELISA and for clone 17 with Western Blot.

Statistical Analyses:

Statistical analysis was performed with two-tailed unpaired Students *t* test, p values<0.05 were considered statistically significant. For in vitro experiments, each lead antibody was compared directly to its appropriate control. For in vivo experiments, each lead antibody was directly compared with Ctrl-Fc to determine significance of brain uptake.

Results:

Phage display screening using iPSC-derived BMEC model

A major challenge in phenotypic screens for antibodies capable of transcytosing the BBB is the inherent paracellular leakiness of many BBB models. In the setting of a two compartment barrier model where a phage display antibody library is added to the blood side compartment (Fig. 1A, **Step 3**), paracellular leakiness will result in significant non-

specific phage recovery in the brain side compartment masking potentially valuable, rare clones that actually had to traverse the BMECs by RMT. To address this longstanding challenge, we employed an iPSC-derived BMEC BBB model that combines the advantages of human-sourced material with robust barrier properties (19), which could in principle limit non-specific phage recovery. These BMECs express a collection of markers expressed by the BBB and a host of transporter proteins including nutrient transporters, drug efflux transporters, and large molecule RMT systems (18, 19) suggesting they could also be well-suited for transporter-based screening (25, 33). Indeed, when irrelevant phage were applied to iPSC-derived BMEC monolayers varying in barrier quality as assessed by transendothelial electrical resistance (TEER), it was discovered that non-specific phage passage into the bottom well was very high in the traditional BBB model TEER range of 100–200 ohm-cm^2 (Table 1). However, the irrelevant phage transport was greatly reduced above approximately 1000 ohm-cm^2, a range uniquely achieved by the human iPSC-based system. Thus, to avoid a large and deleterious background of phage, we used BMECs having a barrier of at least 1000 ohm-cm^2 for the transcytosis component of our screening procedure.

The entire screening procedure is illustrated in Fig. 1A. A library of 5×10^8 nonimmune human-derived scFvs displayed on the surface of fd-tet phage (26) was used for screening as multivalent display can help bias the screen towards antibodies capable of internalization (34), a requirement for transcytosis. First, a library pre-subtraction step was performed on human lung and heart endothelial cells (Fig. 1A, Step 1) in an attempt to de-enrich phage binding to common endothelial antigens and thereby gain BBB selectivity, as transcriptomics studies have shown a reasonably close relation between lung and heart cells to the BBB (35). Next, three screening rounds of BMEC binding and internalization were performed in order to enrich for scFvs having binding and internalization capacity, and to increase oversampling of such clones for the stringent transcytosis round. For these three rounds, 10^{11} phage from the presubtracted pool were incubated on BMECs, first on ice as a binding step and then at 37 °C to allow for phage internalization (Fig. 1A, Step 2). The surface of the BMEC monolayer was subsequently stripped of phage particles with low pH washes, cells were lysed, and internalized phage recovered in bacteria. After three rounds of binding and internalization, the phage pools were substantially enriched for BMEC-binding scFvs as measured by flow cytometry with the recovered phage pools (Fig. 1B). Next, in order to identify scFv-displaying phage capable of transcytosis across the BMEC monolayers, internalizing phage pools were added to the upper chamber of BMECs in a Transwell system and allowed to transcytose for 3 hours before phage recovery from the bottom chamber (Fig. 1A, Step 3i). A total of 220 phage clones were isolated from the bottom chamber (out of 10^{11} phage added), indicating the stringency of the screen. Phage immunochemistry on BMEC monolayers was performed to identify antibodies that truly interact with BMECs as opposed to non-specific phage that leaked through the monolayer, despite its substantial barrier (Fig. 1C). Upon sequencing, 12 unique scFvs were capable of binding to BMECs in phage display format. Moreover, it was observed that two clones, named 3 and 22Ch, represented >60% of the transcytosing phage pool (142/220 sequences, Supplemental Table S1). When 22Ch-displaying phage were reapplied to the Transwell set-up, they were transported across the BMEC monolayer to a greater extent (~6-fold) than

non-specific phage without affecting barrier properties, indicating that the screen can indeed discriminate transcytosing phage (Supplemental Fig. S1). However, since there was a prevalence of the two clones, 22Ch and 3, they could potentially mask the screen diversity by saturating the BMEC transcytosis capacity. Thus, to expand the diversity of scFvs recovered, scFv clones 3 and 22Ch were produced as soluble proteins and used to perform a competitive transcytosis screen. Soluble scFvs at saturating conditions were added to the upper chamber along with the internalizing phage antibody pools to reduce the interactions between phage displaying scFvs 3 and 22Ch and BMECs (Fig. 1A, step 3ii, and Materials and Methods). Individual phage clones accumulating in the bottom chamber were isolated and sequenced. Neither clone 3 nor 22Ch was found in the transcytosed fraction following soluble scFv competition, and the competitive transcytosis approach resulted in 10 more unique scFvs that bound to BMECs in phage display format, for a total of 22 lead scFvs.

ScFvs internalize into BMECs and bind to human and mouse brain microvessels

BMEC-binding scFvs identified from the transcytosis rounds were subcloned, bacterially expressed and purified. A total of 15 of the 22 scFvs could be produced at levels allowing downstream evaluation. After pulsing soluble scFvs onto BMECs, 12 out of the 15 scFvs bound to BMECs, with 10 also exhibiting clear internalization into BMECs (Table 2 and Supplemental Fig. S2). For further evaluation, scFvs were reformatted as scFv-Fc fusions, expressed in HEK293F cells and purified (Fig. 2A). Six clones (3, 9, 26, 17, 46.1 and 22Ch) were produced in sufficient amounts for *in vitro* evaluation and subsequent *in vivo* assessment. As expected, scFv-Fc formatted antibodies migrated as dimers of ~100kDa under non-reducing conditions (Fig. 2B). Apparent affinity (K_D) of scFv-Fcs for binding to BMEC monolayers was determined and ranged from 20–200nM (Table 3). To confirm that the reformatted scFv-Fc fusions retained their ability to bind and internalize into BMECs, scFv-Fcs were applied to BMECs. Each of the 6 assayed scFv-Fcs preserved their capacity to bind and internalize into BMECs (Fig. 2C). Five of six antibodies showed a similar binding and internalization appearance (clones 3, 9, 17, 22Ch, and 26). The surface bound antibodies were distributed across the BMEC surface (Fig. 2C, red), with the internalized antibodies found in puncta that were often perinuclear (Fig. 2C, green), reminiscent of intracellular vesicles. In striking contrast, the major fraction of internalized 46.1-scFv-Fc trafficked to the cell-cell junctions. Quantitative internalization assays were performed with BMEC monolayers and 5 out of 6 clones tested exhibited a statistically significant, temperature dependent internalization, suggestive of endocytosis processes (Fig. 2D).

Given the differences in the intracellular distribution of clone 46.1 after internalization into iPSC-derived BMECs, we sought to determine its intracellular localization with respect to the apical (“blood-side”) tight junction associated protein ZO-1 and the basolateral (“brain-side”) protein, CD31 (Supplemental Fig. S3). BMECs were incubated with 46.1-scFv-Fc and clone 46.1 trafficked to the cell-cell junctions within 15 min of internalization (Supplemental Fig. S3A). The spatial distribution of clone 46.1 was next resolved in a series of confocal images spanning the cell monolayer. Whereas the surface bound 46.1 was found apical to ZO-1, the internalized 46.1 was instead found in a position that was basolateral to ZO-1 (Supplemental Fig. S3, B and C), and in the same focal plane with CD31 on the “brain

side" of BMECs (Supplemental Fig. S3D). Thus, clone 46.1 relatively rapidly transports from the apical membrane to the basolateral junctional membrane in BMECs.

Since *in vitro* modeling of the BBB can result in altered expression of surface receptors (36), the *in vivo* relevance in terms of the capacity of the identified antibodies to bind the BBB in brain tissue was next explored. First, the binding of scFvs to human brain sections was evaluated. Ten of twelve antibodies bind to their cognate antigens on human brain microvessels in tissue sections (Fig. 2E and Table 2). Given the need to perform pre-clinical evaluation, we also tested the antibody crossreactivity to mouse BBB antigens. Of the 10 scFvs with BBB binding in human sections, 9 also bound the mouse BBB (Fig. 2E and Table 2). Only those clones that could be produced in reasonable yields as scFv-Fcs and exhibited BMEC internalization and binding to both human and mouse BBB were evaluated further (3, 9, 26, 17, 46.1 and 22Ch).

Antibodies accumulate in brain microvessels and parenchyma after intravenous administration in mice

The scFv-Fcs that showed binding to brain microvessels in both human and mouse brain sections were next tested for brain targeting after intravenous administration. Mice were administered an intravenous scFv-Fc dose of 5 mg/kg, and the antibodies were allowed to circulate for 1 hour. The unbound antibody fraction was cleared from the blood vessels by whole body perfusion with a physiological saline solution. Perfusate also contained a fluorescently labeled lectin to visualize the lumen of the blood vessels. Following fixation, whole brains were removed and examined by immunohistochemistry. Immunohistochemical analysis of brain sections revealed that four of five injected antibodies target luminal BBB antigens (3, 17, 26 and 46.1, Fig. 3A). Clones 3-, 26- and 46.1-scFv-Fcs are visible as punctate structures (Fig. 3A, white arrows) resembling endocytic vesicles, suggesting receptor-mediated uptake in brain endothelial cells *in vivo*, while for clone 17, vascular labeling was slightly more diffuse (Fig. 3A). In addition, postvascular antibody was detected in 46.1 injected mice in perivascular processes associated with blood vessels (Fig. 3A, yellow arrow).

Given the appearance of transport through BBB endothelial cells, we further evaluated the antibody localization by confocal microscopy and co-localization with BBB basement membrane component, collagen IV (37), as an indicator of antibody transport from the blood side of the BBB endothelial cells to the brain side of the endothelial cells. Three dimensional reconstructions of confocal Z-stack images indicated that three of the analyzed antibodies (3, 26 and 46.1) exhibit at least partial co-localization with the collagen IV, indicating antibody trafficking to the brain side of the BBB endothelium (Fig. 3B, white arrows, purple merge). By contrast, clone 17 does not exhibit co-localization with collagen IV, but it was consistently detected above background in the postvascular tissue and with some perinuclear localization associated with postvascular cells (Fig. 3B, yellow arrow).

As mentioned above, we frequently observed clone 46.1 in postvascular processes proximal to the microvessels (e.g. Fig. 3A, yellow arrows). To determine the cellular origin of these processes, we next labeled mouse brain sections with the astrocyte marker, glial fibrillary acidic protein (GFAP) (Fig. 3C). Clone 46.1 could be clearly identified as puncta associated

with GFAP+ astrocyte processes (Fig. 3C). Astrocytes positive for 46.1-scFv-Fc were unevenly spread throughout the sagittal sections analyzed, with a tendency to occur most frequently in the hippocampal region. Other, unidentified CNS cells of non-vascular origin, also likely accumulate clone 46.1 (Fig. 3C, yellow arrow). Taken together, immunofluorescence suggests that clones 17 and 46.1 traffic across the BBB, with clone 46.1 exhibiting demonstrable postvascular association with perivascular astrocytes.

Given the capacity for clones 17 and 46.1 to cross the BBB, we investigated if they recognize the well-studied transferrin (TfR) or insulin receptors (IR). A competitive binding assay was used to determine if the scFv-Fcs interact substantially with TfR or IR by pre-incubating scFv-Fcs with excess recombinant receptor ectodomains before a cell surface binding assay. Cell surface binding of both clones 46.1 and 17 was not substantially reduced by either of the competing ligands (Supplemental Fig. S4). Although there was a small decrease in both 17 and 46.1 binding in the presence of IR competition, it was quite small in comparison with the 80% reduction observed when anti-human IR control antibody was competed by soluble IR ectodomain. These data, along with the different trafficking patterns observed for 17 and 46.1, indicate that these two scFvs are not targeting TfR or IR.

Antibodies have variable biodistributions after intravenous administration

Given the pre-subtraction step that was built into the screen design (Fig. 1A), we also wished to assess the potential brain selectivity of candidate antibodies. To this end, antibody uptake was qualitatively assessed using immunohistochemistry. Antibody localization in heart and lung as highly vascularized organs as well as in liver and kidney as major clearance organs was assessed. Cervical and thoracic segments from the spinal cord were additionally analyzed for presence of antibodies. The qualitative analysis of organ biodistribution is summarized in Table 4 and representative images for the clones are shown in Fig. 4 and Supplemental Fig. S5. Albeit with differences in tissue-specific cellular distribution, clone 3 and 17 were found in all analyzed organs. In contrast, clone 26 was not detected in heart, lung or kidney tissue (Supplemental Fig. S5). Clone 46.1 was not detected in heart microvasculature, showing at least partial selectivity to brain microvessels. Of particular interest with clone 46.1 was its cellular localization in liver and kidney, which suggested transcellular junctional trafficking in these organs. For instance, hepatocytes, like BBB endothelial cells, are polarized, with apical and basolateral membrane, segregated by tight junctions (38). Clone 46.1 could be found localizing at the cell-cell junctions of hepatocytes (Fig. 4, white arrow). In addition, clone 46.1 could be found clearly localized at the cell-cell junctions of kidney tubular epithelial cells (Fig. 4, yellow arrow). Although clone 46.1 has a junctional appearance after intracellular trafficking, it does not appear to cause any BBB disruption as no vascular leakage of the perfused lectin tracer was found in brain, while the tracer could be found around the leaky vessels in the liver and kidney (Fig 4. and Supplemental Fig. S6). Finally, we sought to determine whether antibodies could accumulate in the spinal cord. Clones 3, 9, 17 and 46.1 were found within the endothelial cells of capillaries penetrating the spinal cord, despite the fact that clone 9 did not bind BBB microvessels. Overall, the variable organ and tissue distribution of candidate antibodies points to different receptors engaged in their uptake and transport on both organ and cellular levels.

Quantification of scFv-Fc brain accumulation after intravenous administration

Given the immunofluorescence analyses that indicated postvascular brain accumulation of clones 17 and 46.1, we further quantified their accumulation in whole mouse brain after intravenous administration. ScFv-Fcs at 20 mg/kg were injected and allowed to circulate for 1 hour. After whole body perfusion to remove the unbound antibodies from the vasculature, brains were isolated, homogenized and antibodies extracted. The concentration of antibodies in brain extracts (vascular-associated and parenchymal) was determined with ELISA (Fig. 5). The measured concentration of clone 46.1 (8.1± 1.2 nM) was 26-fold higher than that for negative control-Fc (0.31 ± 0.11 nM). Clone 17 also accumulated in brain (2.79 ± 0.63 nM), about 9-fold higher than control. Additionally, the antibody concentration in the terminal plasma was measured, and the brain concentrations were also expressed as a ratio to the plasma concentration (Table 5), again indicating the selective uptake of clones 46.1 (0.72%) and 17 (0.28 %) in the brain versus control (0.015%).

Discussion:

In this study, we developed an original antibody screening strategy to identify antibodies that target human BBB antigens and also target and transcytose the murine BBB after systemic administration. Our functional screening strategy employed iPSC-derived BMEC-like cells as a screening substrate. Importantly, the paracellular tightness of this BBB model was key to limit the nonspecific accumulation of phage in the lower chamber, which would mask the recovery of clones that could truly transcytose across the BMECs. This stringent screening filter allowed for the identification of a panel of scFvs that upon further characterization led to a set of lead molecules capable of targeting and trafficking at the BBB in vivo. Although the iPSC-based BMEC-like model has been shown to have reasonable fidelity in modeling many BBB transport attributes (18, 19, 33), it cannot fully replicate all BBB functions (17, 20, 39). However, 10 of the 12 scFvs which bound to the BMECs also bound to the human BBB in tissue sections. By contrast, other screens using immortalized or primary BMEC substrates yield very few antibodies having in vivo relevance (29, 40). While the screening paradigm also included a pre-subtraction step on human lung and heart endothelial cells in an attempt to bias the screen towards BBB-selective antibodies, the biodistribution analyses indicated that the antibodies had a range of tissue selectivities. These data mirror other in vitro screening outcomes where pre-subtraction methods gave minimal advantage for *in vivo* selectivity of the lead molecules (15, 29, 34, 41, 42). These findings support the validity of the iPSC-BMEC system as a screening substrate, and along with the barrier properties of the model, the strategies described here may facilitate future efforts in identifying and engineering additional antibody-BBB transporter combinations.

Most of the scFvs (9 of 12) that were identified as binding to BMECs, also internalized, indicating that the internalization and transcytosis screening steps were enriching for endocytosing antibody-receptor combinations. The percentage of internalizing antibodies was much higher than other BBB screens using phage or yeast display libraries (29, 40). ScFvs interacted with the BMECs in a temperature-dependent fashion, and were found in intracellular punctae, suggesting RMT as the predominant route for cellular uptake. In particular, scFv 46.1 had a unique uptake pattern, namely there were few cytoplasmic 46.1-

containing structures and most antibody could be found in punctae at the cell-cell junctions, seemingly distinct from recycling or degradative compartments typical of targeted BBB receptors like the TfR (43, 44). Moreover, confocal microscopy indicated the rapid, vectorial transport of 46.1 from the apical membrane to the basolateral junctions. While the identification of the receptor targeted by 46.1 and the elucidation of the detailed intracellular transport mechanism are the focus of future work, we have not observed any literature describing such an antibody transport profile at the BBB. In addition to this unique intracellular distribution of internalized antibody, receptor ectodomain competition experiments indicated that the RMT target is not the transferrin or insulin receptors, suggesting that the 46.1-receptor system represents a new potential platform for brain delivery. As previously examined for the TfR (7) and basigin receptors (11), the effects of the 46.1 antibody on the function and regulation of the targeted receptor will also be important as the 46.1-receptor system is further evaluated.

The potential of these new antibody-receptor pairs was further confirmed *in vivo* after intravenous administration. Four of five scFv-Fcs accumulated in mouse brain endothelium after one hour of circulation. Clones 3, 26 and 46.1 yielded a clear intracellular vesicular localization along the brain microvessels. Through collagen IV colocalization, it was apparent that each of these clones was also trafficked to the brain side of the brain endothelial cells. Once an antibody leaves the vasculature, it undergoes a rapid 1000-fold dilution which hampers downstream postvascular detection (45). However, if the antibody also binds to a postvascular cell like an astrocyte or neuron, it re-concentrates and can be readily detected (46, 47). In this way, it was possible to observe the postvascular accumulation of clone 46.1 where it was found associated with GFAP+ astrocyte foot processes and cell bodies. In addition, 46.1 was detected as punctae in GFAP- brain cells in the vicinity of 46.1-containing astrocytes. These key findings gave clear evidence of full transcytosis of clone 46.1 across the BBB and its distribution in the brain parenchyma, a critical first step in preclinical evaluation. Clone 17 did not co-localize with the vascular basement membrane. However, it could be observed reproducibly above background within the postvascular tissue compartment with occasional perinuclear association. Although not as clear as the 46.1 association with GFAP+ astrocytes, clone 17 also offers promise as a new antibody-receptor combination.

To benchmark the brain accumulation of clones 17 and 46.1, we next quantified the amount of antibody reaching the brain. After intravenous administration at 20 mg/kg, and one hour of circulation time, the brain concentration of clone 46.1 (8.1 nM, 0.72% brain/plasma) was 26-fold higher than control, and 9-fold higher for clone 17 (2.8 nM, 0.28% brain/plasma), respectively. These brain uptake levels are comparable to brain concentrations previously reported for engineered anti-transferrin antibodies (47–49). As in these comparative studies, the brain extracts were prepared from the whole tissue, including both the antibody in the brain parenchyma and that sequestered in the blood vessels endothelium. Combined with our immunofluorescence data, it is clear that within the one hour time window, at least some of the administered antibody is accumulating in postvascular brain tissue. Ultimately, antibody uptake levels are controlled by myriad factors (50) including antigen binding in non-target tissue, dose limitations, antibody affinity and avidity (6, 7, 44, 48, 51). For instance, given the fairly broad, but specific peripheral localization of 46.1 into lung, liver and kidney cells,

the specificity and potency of conjugated drug payload will be a key consideration. Other BBB antibodies under development that target ubiquitously expressed receptors, including the TfR, also face similar challenges where payload choice and protein engineering need to be combined to maximize efficacy (7, 46, 49). Thus, antibody and payload engineering strategies will be important for the further development of the new antibody-receptor systems described here. In summary, we have identified new and promising antibodies that show substantial brain uptake, including postvascular accumulation. Importantly for translational considerations, our antibodies demonstrate cross-reactivity to mouse and human antigens. This work should enable the development of these lead antibodies as a platform to deliver therapeutics to the brain.

Supplementary Material

Refer to Web version on PubMed Central for supplementary material.

Acknowledgments:

We would like to thank Dr. James D. Marks for the kind gift of phage display scFv library and Lance Rodenkirch for help with X-Clarity tissue preparation. This work was supported in part by National Institutes of Health grant NS071513 and Defense Threat Reduction Agency grant HDTRA1-15-1-0012.

Abbreviations

BBB	blood–brain barrier
BMECs	brain microvascular endothelial cells
RMT	receptor-mediated transcytosis
iPSC	induced pluripotent stem cell
scFv	single-chain variable fragment
scFv-Fc	single-chain variable fragment fused to constant Fc region
TEER	transendothelial electrical resistance
TfR	transferrin receptor
IR	insulin receptor
hLECs	human lung microvascular endothelial cells
hCECs	human heart microvascular endothelial cells
CFU	colony forming units
rhTfR	recombinant human transferrin receptor ecto-domain
rIR	recombinant insulin receptor ecto-domain
GFAP	glial fibrillary acidic protein

References:

1. Abbott NJ and Friedman A (2012) Overview and introduction: the blood-brain barrier in health and disease. Epilepsia 53 Suppl 6, 1–6
2. Poduslo JF, Curran GL, and Berg CT (1994) Macromolecular permeability across the blood-nerve and blood-brain barriers. Proc. Natl. Acad. Sci. U. S. A 91, 5705–5709 [PubMed: 8202551]
3. Jones AR and Shusta EV (2007) Blood-brain barrier transport of therapeutics via receptor-mediation. Pharm. Res 24, 1759–1771 [PubMed: 17619996]
4. Pardridge WM, Kang YS, and Buciak JL (1994) Transport of human recombinant brain-derived neurotrophic factor ({BDNF}) through the rat blood-brain barrier in vivo using vector-mediated peptide drug delivery. Pharm. Res 11, 738–746 [PubMed: 8058646]
5. Pardridge WM, Kang YS, Buciak JL, and Yang J (1995) Human insulin receptor monoclonal antibody undergoes high affinity binding to human brain capillaries in vitro and rapid transcytosis through the blood-brain barrier in vivo in the primate. Pharm. Res 12, 807–816 [PubMed: 7667183]
6. Niewoehner J, Bohrmann B, Collin L, Urich E, Sade H, Maier P, Rueger P, Stracke JO, Lau W, Tissot AC, Loetscher H, Ghosh A, and Freskgård P-O (2014) Increased brain penetration and potency of a therapeutic antibody using a monovalent molecular shuttle. Neuron 81, 49–60 [PubMed: 24411731]
7. Couch JA, Yu YJ, Zhang Y, Tarrant JM, Fuji RN, Meilandt WJ, Solanoy H, Tong RK, Hoyte K, Luk W, Lu Y, Gadkar K, Prabhu S, Ordonia BA, Nguyen Q, Lin Y, Lin Z, Balazs M, Scearce-Levie K, Ernst JA, Dennis MS, and Watts RJ (2013) Addressing safety liabilities of TfR bispecific antibodies that cross the blood-brain barrier. Sci. Transl. Med 5, 183ra57, 1–12
8. Johnsen KB, Bak M, Melander F, Thomsen MS, Burkhart A, Kempen PJ, Andresen TL, and Moos T (2019) Modulating the antibody density changes the uptake and transport at the blood-brain barrier of both transferrin receptor-targeted gold nanoparticles and liposomal cargo. J. Control. Release 295, 237–249 [PubMed: 30633947]
9. Goulatis LI and Shusta EV (2017) Protein engineering approaches for regulating blood-brain barrier transcytosis. Curr. Opin. Struct. Biol 45, 109–115 [PubMed: 28040636]
10. Stutz CC, Zhang X, and Shusta EV (2014) Combinatorial approaches for the identification of brain drug delivery targets. Curr. Pharm. Des 20, 1564–1576 [PubMed: 23789958]
11. Zuchero YJY, Chen X, Bien-Ly N, Bumbaca D, Tong RK, Gao X, Zhang S, Hoyte K, Luk W, Huntley MA, Phu L, Tan C, Kallop D, Weimer RM, Lu Y, Kirkpatrick DS, Ernst JA, Chih B, Dennis MS, and Watts RJ (2016) Discovery of Novel Blood-Brain Barrier Targets to Enhance Brain Uptake of Therapeutic Antibodies. Neuron 89, 70–82 [PubMed: 26687840]
12. Abulrob A, Sprong H, Van Bergen En Henegouwen P, and Stanimirovic D (2005) The blood-brain barrier transmigrating single domain antibody: Mechanisms of transport and antigenic epitopes in human brain endothelial cells. J. Neurochem 95, 1201–1214 [PubMed: 16271053]
13. Urich E, Schmucki R, Ruderisch N, Kitas E, Certa U, Jacobsen H, Schweitzer C, Bergadano A, Ebeling M, Loetscher H, and Freskgård PO (2015) Cargo Delivery into the Brain by in vivo identified Transport Peptides. Sci. Rep 5, 14104 [PubMed: 26411801]
14. Pasqualini R and Ruoslahti E (1996) Organ targeting in vivo using phage display peptide libraries. Nature 380, 364–366 [PubMed: 8598934]
15. Muruganandam A, Tanha J, Narang S, and Stanimirovic D (2002) Selection of phage-displayed llama single-domain antibodies that transmigrate across human blood-brain barrier endothelium. FASEB J. Off. Publ. Fed. Am. Soc. Exp. Biol 16, 240–242
16. Stutz CC, Georgieva JV, and Shusta EV (2018) Coupling brain perfusion screens and next generation sequencing to identify blood–brain barrier binding antibodies. AIChE J. 64, 4229–4236 [PubMed: 30872841]
17. Vatine GD, Al-Ahmad A, Barriga BK, Svendsen S, Salim A, Garcia L, Garcia VJ, Ho R, Yucer N, Qian T, Lim RG, Wu J, Thompson LM, Spivia WR, Chen Z, Van Eyk J, Palecek SP, Refetoff S, Shusta EV, and Svendsen CN (2017) Modeling Psychomotor Retardation using iPSCs from MCT8-Deficient Patients Indicates a Prominent Role for the Blood-Brain Barrier. Cell Stem Cell 20, 831–843.e5 [PubMed: 28526555]

18. Lippmann ES, Azarin SM, Kay JE, Nessler RA, Wilson HK, Al-Ahmad A, Palecek SP, and Shusta EV (2012) Derivation of blood-brain barrier endothelial cells from human pluripotent stem cells. Nat. Biotechnol 30, 783–791 [PubMed: 22729031]
19. Lippmann ES, Al-Ahmad A, Azarin SM, Palecek SP, and Shusta EV (2014) A retinoic acid-enhanced, multicellular human blood-brain barrier model derived from stem cell sources. Sci. Rep 4, 4160 [PubMed: 24561821]
20. Kurosawa T, Tega Y, Higuchi K, Yamaguchi T, Nakakura T, Mochizuki T, Kusuhara H, Kawabata K, and Deguchi Y (2018) Expression and Functional Characterization of Drug Transporters in Brain Microvascular Endothelial Cells Derived from Human Induced Pluripotent Stem Cells. Mol. Pharm 15, 5546–5555 [PubMed: 30376629]
21. Wang YI, Abaci HE, and Shuler ML (2017) Microfluidic blood–brain barrier model provides in vivo-like barrier properties for drug permeability screening. Biotechnol. Bioeng 114, 184–194 [PubMed: 27399645]
22. Faley SL, Neal EH, Wang JX, Bosworth AM, Weber CM, Balotin KM, Lippmann ES, and Bellan LM (2019) iPSC-Derived Brain Endothelium Exhibits Stable, Long-Term Barrier Function in Perfused Hydrogel Scaffolds. Stem Cell Reports 12, 474–487 [PubMed: 30773484]
23. Campisi M, Shin Y, Osaki T, Hajal C, Chiono V, and Kamm RD (2018) 3D self-organized microvascular model of the human blood-brain barrier with endothelial cells, pericytes and astrocytes. Biomaterials 180, 117–129 [PubMed: 30032046]
24. Park TE, Mustafaoglu N, Herland A, Hasselkus R, Mannix R, FitzGerald EA, Prantil-Baun R, Watters A, Henry O, Benz M, Sanchez H, McCrea HJ, Goumnerova LC, Song HW, Palecek SP, Shusta E, and Ingber DE (2019) Hypoxia-enhanced Blood-Brain Barrier Chip recapitulates human barrier function and shuttling of drugs and antibodies. Nat. Commun 10
25. Ribecco-Lutkiewicz M, Sodja C, Haukenfrers J, Haqqani AS, Ly D, Zachar P, Baumann E, Ball M, Huang J, Rukhlova M, Martina M, Liu Q, Stanimirovic D, Jezierski A, and Bani-Yaghoub M (2018) A novel human induced pluripotent stem cell blood-brain barrier model: Applicability to study antibody-triggered receptor-mediated transcytosis. Sci. Rep 8, 1873 [PubMed: 29382846]
26. Sheets MD, Amersdorfer P, Finnern R, Sargent P, Lindquist E, Schier R, Hemingsen G, Wong C, Gerhart JC, Marks JD, and Lindqvist E (1998) Efficient construction of a large nonimmune phage antibody library: the production of high-affinity human single-chain antibodies to protein antigens. Proc. Natl. Acad. Sci. U. S. A 95, 6157–6162 [PubMed: 9600934]
27. O'Connell D, Becerril B, Roy-Burman A, Daws M, and Marks JD (2002) Phage versus Phagemid Libraries for Generation of Human Monoclonal Antibodies. J. Mol. Biol 321, 49–56 [PubMed: 12139932]
28. Zhou Y and Marks JD (2009) Identification of Target and Function Specific Antibodies for Effective Drug Delivery. In Methods in molecular biology (Clifton, N.J.) vol. 525, pp. 145–160,
29. Jones AR, Stutz CC, Zhou Y, Marks JD, and Shusta EV (2014) Identifying blood-brain-barrier selective single-chain antibody fragments. Biotechnol. J 9, 664–674 [PubMed: 24644233]
30. Umlauf BJ, Clark PA, Lajoie JM, Georgieva JV, Bremner S, Herrin BR, Kuo JS, and Shusta EV (2019) Identification of variable lymphocyte receptors that can target therapeutics to pathologically exposed brain extracellular matrix. Sci. Adv 5
31. Han BW, Herrin BR, Cooper MD, and Wilson IA (2008) Antigen recognition by variable lymphocyte receptors. Science (80-.) 321, 1834–1837
32. Stephen TL, Tamagnini F, Piegsa J, Sung K, Harvey J, Oliver-Evans A, Murray TK, Ahmed Z, Hutton ML, Randall A, O'Neill MJ, and Jackson JS (2019) Imbalance in the response of pre- and post-synaptic components to amyloidopathy. Sci. Rep 9
33. Stebbins MJ, Wilson HK, Canfield SG, Qian T, Palecek SP, and Shusta EV (2016) Differentiation and characterization of human pluripotent stem cell-derived brain microvascular endothelial cells. Methods 101, 93–102 [PubMed: 26518252]
34. Poul MA, Becerril B, Nielsen UB, Morisson P, and Marks JD (2000) Selection of tumor-specific internalizing human antibodies from phage libraries. J. Mol. Biol 301, 1149–1161 [PubMed: 10966812]
35. Nolan DJ, Ginsberg M, Israely E, Palikuqi B, Poulos MG, James D, Ding B-S, Schachterle W, Liu Y, Rosenwaks Z, Butler JM, Xiang J, Rafii A, Shido K, Rabbany SY, Elemento O, and Rafii S

(2013) Molecular signatures of tissue-specific microvascular endothelial cell heterogeneity in organ maintenance and regeneration. Dev. Cell 26, 204–219 [PubMed: 23871589]

36. Helms HC, Abbott NJ, Burek M, Cecchelli R, Couraud P-O, Deli MA, Förster C, Galla HJ, Romero IA, Shusta EV, Stebbins MJ, Vandenhaute E, Weksler B, and Brodin B (2016) In vitro models of the blood–brain barrier: An overview of commonly used brain endothelial cell culture models and guidelines for their use. J. Cereb. Blood Flow Metab 36, 862–890 [PubMed: 26868179]
37. Kühn K (1995) Basement membrane (type IV) collagen. Matrix Biol. 14, 439–445 [PubMed: 7795882]
38. Wang L and Boyer JL (2004) The maintenance and generation of membrane polarity in hepatocytes. Hepatology 39, 892–899 [PubMed: 15057889]
39. Delsing L, Dönnes P, Sánchez J, Clausen M, Voulgaris D, Falk A, Herland A, Brolén G, Zetterberg H, Hicks R, and Synnergren J (2018) Barrier Properties and Transcriptome Expression in Human iPSC-Derived Models of the Blood–Brain Barrier. Stem Cells 36, 1816–1827 [PubMed: 30171748]
40. Wang XX, Cho YK, and Shusta EV (2007) Mining a yeast library for brain endothelial cell-binding antibodies. Nat. Methods 4, 143–145 [PubMed: 17206151]
41. Li J, Feng L, Fan L, Zha Y, Guo L, Zhang Q, Chen J, Pang Z, Wang Y, Jiang X, Yang VC, and Wen L (2011) Targeting the brain with PEG-PLGA nanoparticles modified with phage-displayed peptides. Biomaterials 32, 4943–4950 [PubMed: 21470674]
42. Zorniak M, Clark PA, Umlauf BJ, Cho Y, Shusta EV, and Kuo JS (2017) Yeast display biopanning identifies human antibodies targeting glioblastoma stem-like cells. Sci. Rep 7, 15840 [PubMed: 29158489]
43. Ullrich O, Reinsch S, Urbé S, Zerial M, and Parton RG (1996) Rab11 regulates recycling through the pericentriolar recycling endosome. J. Cell Biol 135, 913–924 [PubMed: 8922376]
44. Haqqani AS, Thom G, Burrell M, Delaney CE, Brunette E, Baumann E, Sodja C, Jezierski A, Webster C, and Stanimirovic DB (2018) Intracellular sorting and transcytosis of the rat transferrin receptor antibody {OX}26 across the blood-brain barrier in vitro is dependent on its binding affinity. J. Neurochem
45. Pardridge WM (2015) Blood-brain barrier drug delivery of IgG fusion proteins with a transferrin receptor monoclonal antibody. Expert Opin. Drug Deliv 12, 207–222 [PubMed: 25138991]
46. Yu YJ, Atwal JK, Zhang Y, Tong RK, Wildsmith KR, Tan C, Bien-Ly N, Hersom M, Maloney JA, Meilandt WJ, Bumbaca D, Gadkar K, Hoyte K, Luk W, Lu Y, Ernst JA, Scearce-Levie K, Couch JA, Dennis MS, and Watts RJ (2014) Therapeutic bispecific antibodies cross the blood-brain barrier in nonhuman primates. Sci. Transl. Med 6, 261ra154
47. Webster CI, Caram-Salas N, Haqqani AS, Thom G, Brown L, Rennie K, Yogi A, Costain W, Brunette E, and Stanimirovic DB (2016) Brain penetration, target engagement, and disposition of the blood-brain barrier-crossing bispecific antibody antagonist of metabotropic glutamate receptor type 1. FASEB J. 30, 1927–1940 [PubMed: 26839377]
48. Yu YJ, Zhang Y, Kenrick M, Hoyte K, Luk W, Lu Y, Atwal J, Elliott JM, Prabhu S, Watts RJ, and Dennis MS (2011) Boosting brain uptake of a therapeutic antibody by reducing its affinity for a transcytosis target. Sci. Transl. Med 3, 84ra44
49. Karaoglu Hanzatian D, Schwartz A, Gizatullin F, Erickson J, Deng K, Villanueva R, Stedman C, Harris C, Ghayur T, and Goodearl A (2018) Brain uptake of multivalent and multi-specific DVD-Ig proteins after systemic administration. MAbs 10, 765–777 [PubMed: 29771629]
50. Takakura Y and Hashida M (1996) Macromolecular carrier systems for targeted drug delivery: Pharmacokinetic considerations on biodistribution. Pharm. Res 13, 820–831 [PubMed: 8792417]
51. Farrington GK, Caram-Salas N, Haqqani AS, Brunette E, Eldredge J, Pepinsky B, Antognetti G, Baumann E, Ding W, Garber E, Jiang S, Delaney C, Boileau E, Sisk WP, and Stanimirovic DB (2014) A novel platform for engineering blood-brain barrier-crossing bispecific biologics. FASEB J. 28, 4764–4778 [PubMed: 25070367]

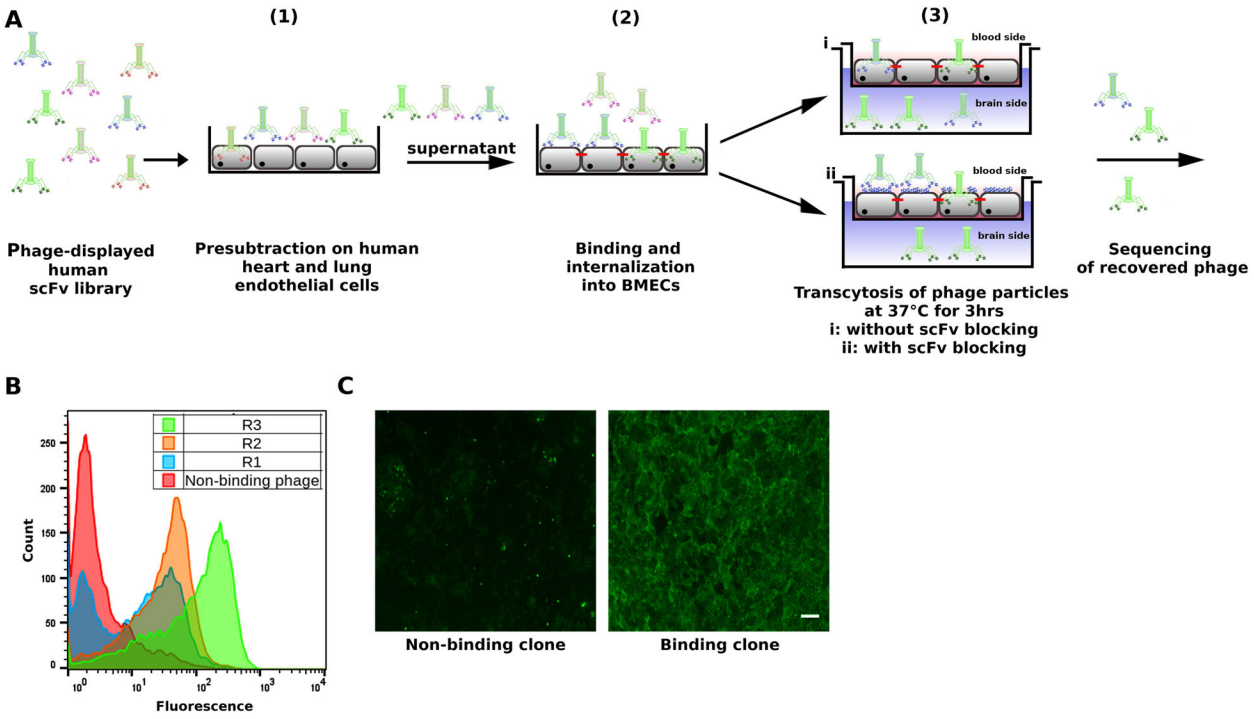

Figure 1.

Antibody library screening on *in vitro* BBB model. *A*) Scheme for the phage display screen. Step 1: pre-subtraction of phage scFv library on cultured human heart and lung endothelial cells in an effort to promote brain selectivity. Step 2: Supernatant from pre-subtraction step is next incubated with iPSC-derived BMECs to allow for binding and internalization of the antibody bearing phage. The antibody pools underwent three rounds of Step 2 internalization screening. Step 3: Internalizing phage were next dosed onto the blood side of BMECs in a Transwell format for 3 hours to allow for transcytosis. Recovered scFv-bearing phage particles were subjected to further analysis. *B*) Enrichment of BMEC-binding phage displayed scFvs as observed by FACS-analysis of phage antibody pools during screening Step 2. Shown are representative histograms of BMECs labeled with phage-displayed scFvs after respective screening rounds. The number of cells (counts: Y-axis) is given as function of the fluorescence intensity of phage antibody labeling of the cells (X-axis). In all experiments, BMECs were incubated with phage antibody pools, and cell-binding was detected by anti-M13 antibody. Geometric means are round R3 – 80.6, R2 – 27, R1 – 10.9, Non-binding phage – 3.16, respectively. *C*) Representative images from clonal phage immunocytochemistry with BMECs to determine clones displaying a BMEC binding phenotype. Scale bar, 50μm. For panels *B*) and *C*) Non-binding phage displays antibotulinum neurotoxin scFv.

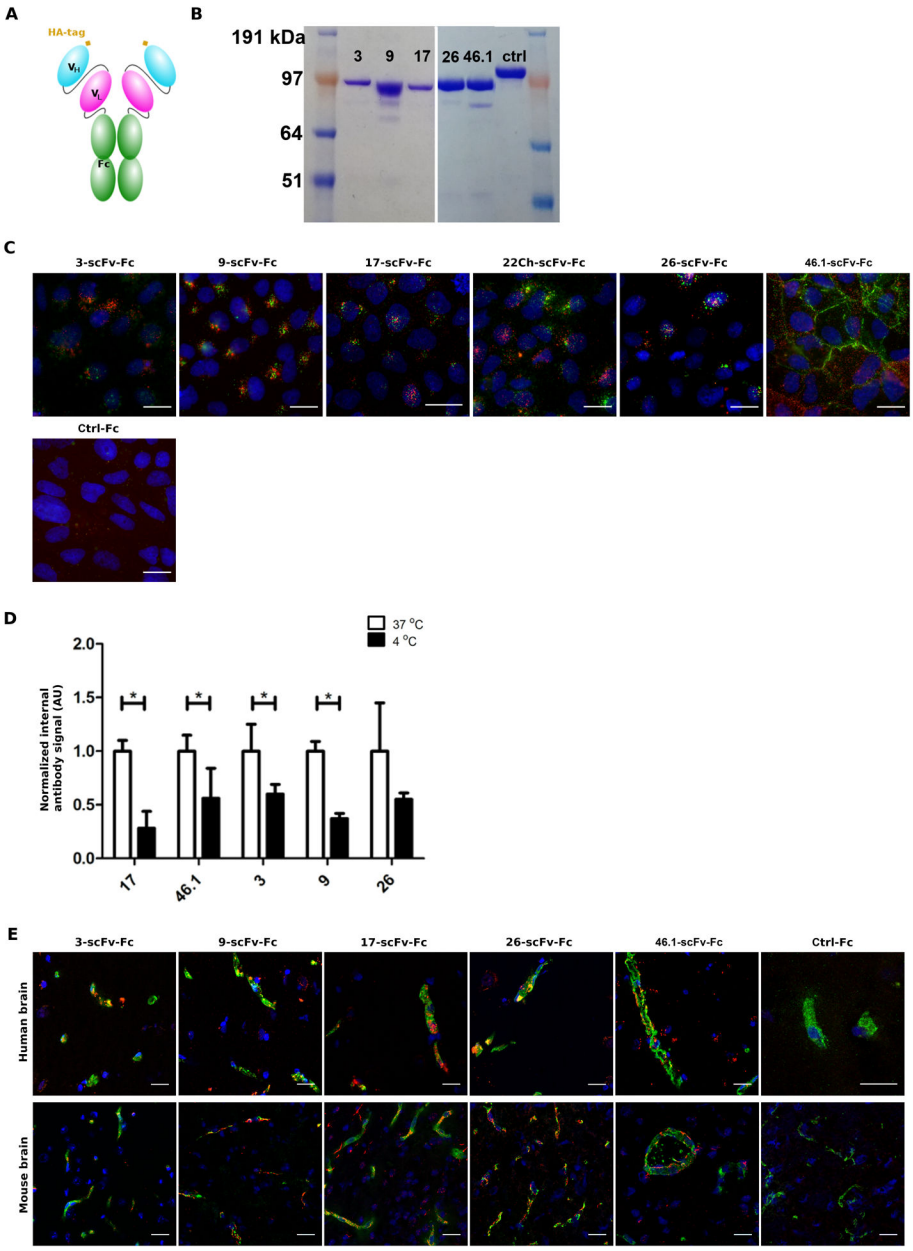

Figure 2.

Antibody binding properties. *A*) ScFv-Fc construct with scFv linked directly to rabbit IgG Fc region. *B*) Non-reducing, Coomassie blue-stained SDS-PAGE gel analysis of scFv-Fc antibodies following expression in HEK293F cells and protein A/G purification. Molecular weights are indicated. *C*) Binding and internalization of antibodies into BMECs. Live cells were incubated with antibodies (5 μg/ml) at 4°C and subsequently at 37°C for 30 min. The cell membrane was washed with cold buffer and the membrane bound fraction labeled with anti-rabbit Fc AlexaFluor555 antibody (red). After fixation and permeabilization the internalized antibodies were labeled with anti-rabbit Fc AlexaFluor488 antibody (green). Images were taken on an epifluorescent microscope. Scale bar, 20 μm. *D*) Temperature-dependent internalization of antibodies. Internalized antibody fluorescent signal values at

4°C are normalized to the total signal per cell at 37°C. Reported are means ±S.D., n=3, *p<0.05 determined by a two-tailed Student's t-test assuming unequal variance. *E*) ScFv-Fcs binding to human and mouse brain microvessels. Cryosections of human and mouse brain were immunolabeled for CD31 (green) to visualize the blood vessels and incubated with 5 μg/ml scFv-Fcs (red) to identify scFv-Fc binding. Nuclei are visualized in blue. Images were taken on a confocal microscope. Scale bar, 20 μm.

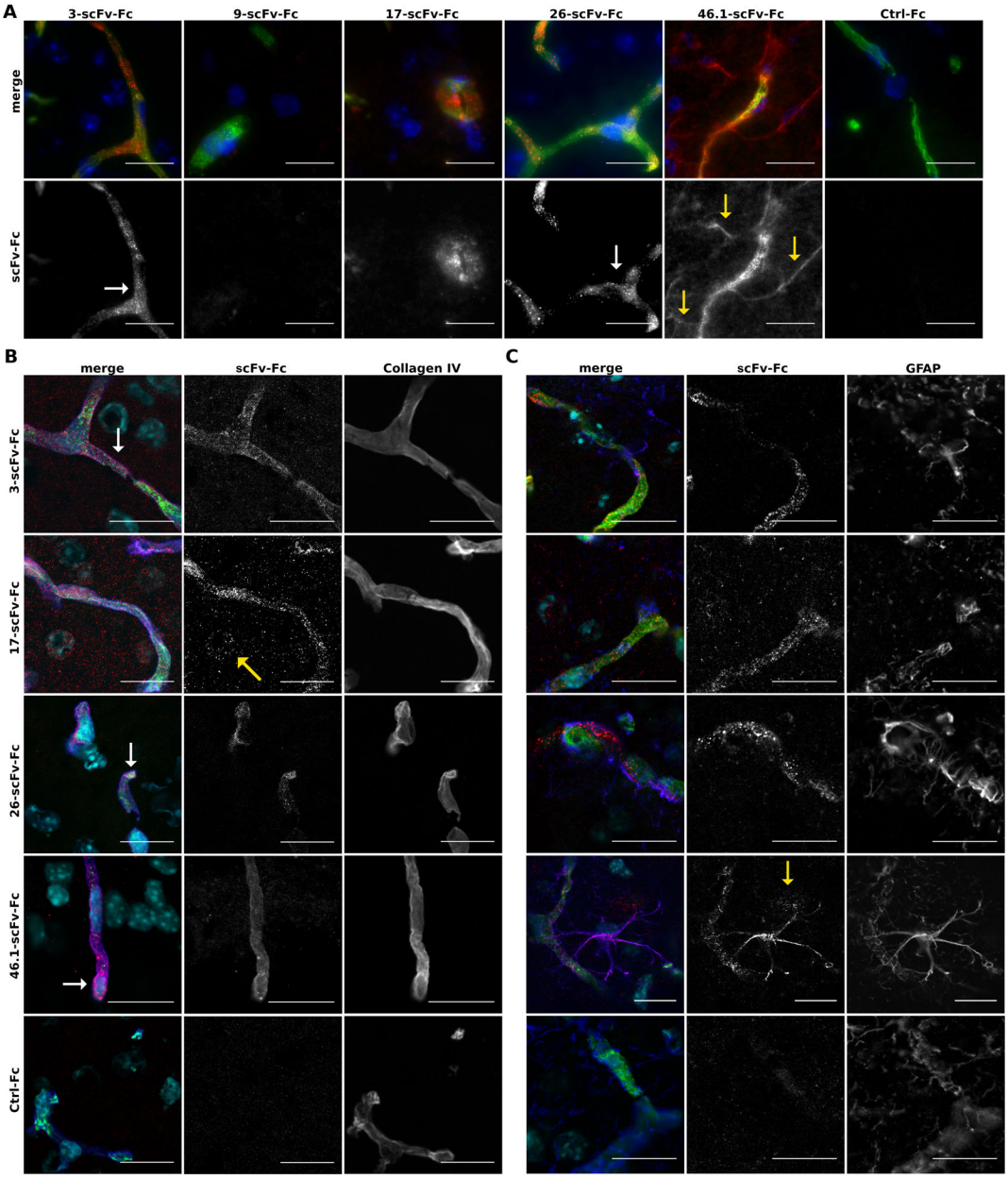

Figure 3.

Brain targeting of antibodies after intravenous administration in mice. *A*) Antibodies (5mg/kg) were injected intravenously in mice. One hour post-injection, mice were whole body perfused and brains collected. ScFv-Fcs (red) were labeled with fluorescent anti-rabbit Fc AlexaFluor555 antibody, blood vessels (green) were visualized with DyLight488 lectin that was present in the perfusion buffer. Four of five analyzed antibodies accumulate in brain vasculature as punctate structures in endothelial cells. Postvascular immunoreactivity was observed in the brain sections from mice injected with clone 46.1 (yellow arrows). Images were taken on an epifluorescence microscope. Scale bar, 20μm. B) Confocal images from a z-stack showing the localization of scFv-Fcs (red) with respect to collagen IV (blue). Blood vessels (green) as in *A*), nuclei (cyan). Clones 3, 26, and 46.1 colocalize with collagen IV

(purple in merge and white arrows). Clone 17 shows no colocalization with collagen IV, but diffuse parenchymal staining was detected. *C*) Co-localization of scFv-Fcs (red) and GFAP+ astrocytes (blue) can be observed in merged confocal images (purple). The yellow arrows in panels *B*) and *C*) indicate accumulation of antibodies in postvascular, GFAP- brain cells. In all panels, the grayscale images are included to assist evaluation of the individual channels depicted in the merged images. Scale bar, 20 μm.

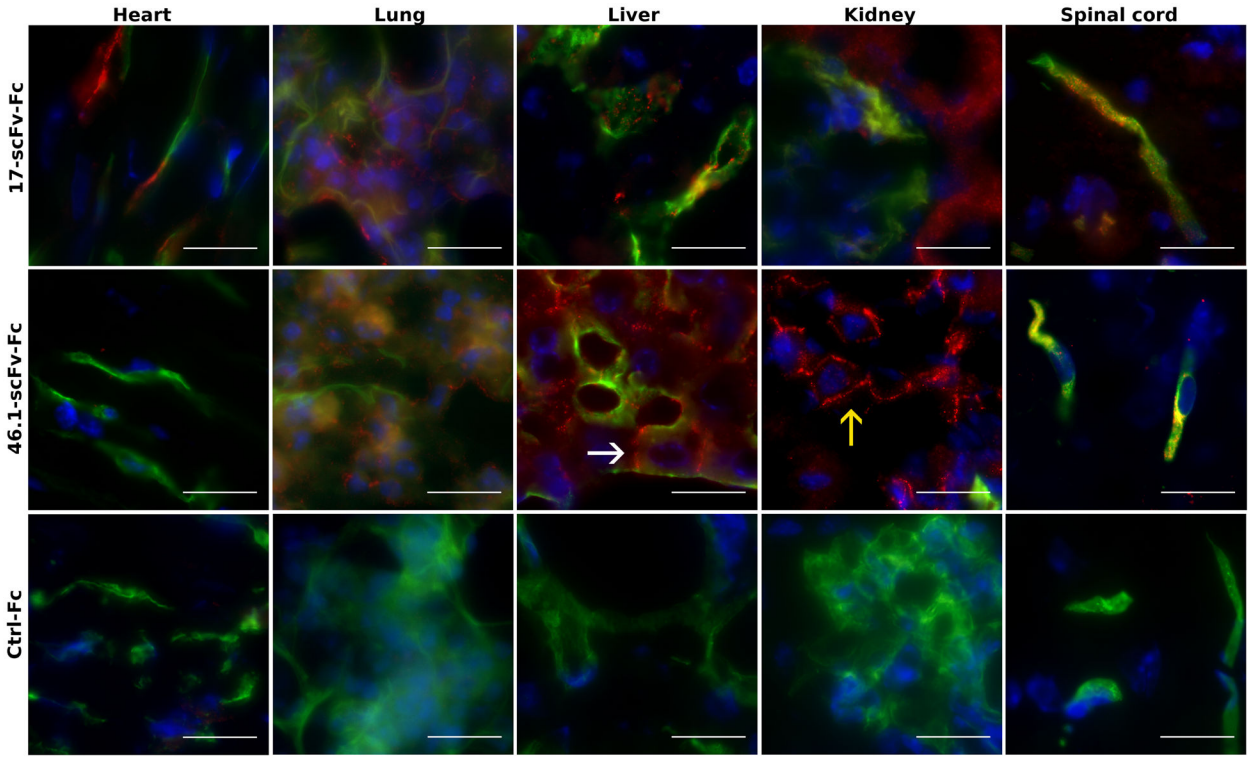

Figure 4.

Organ biodistribution of antibodies. Antibodies (5 mg/kg) were injected intravenously in mice. One hour post-injection, mice were whole body perfused and organs collected. ScFv-Fcs were immunolabeled with fluorescent anti-rabbit Fc AlexaFluor555 antibody (red), blood vessels were visualized with the perfused DyLight488 lectin (green). White and yellow arrows point junctional localization of clone 46.1 in hepatocytes and renal epithelial cells, respectively. Images were taken on an epifluorescence microscope. Scale bar, 20 μm.

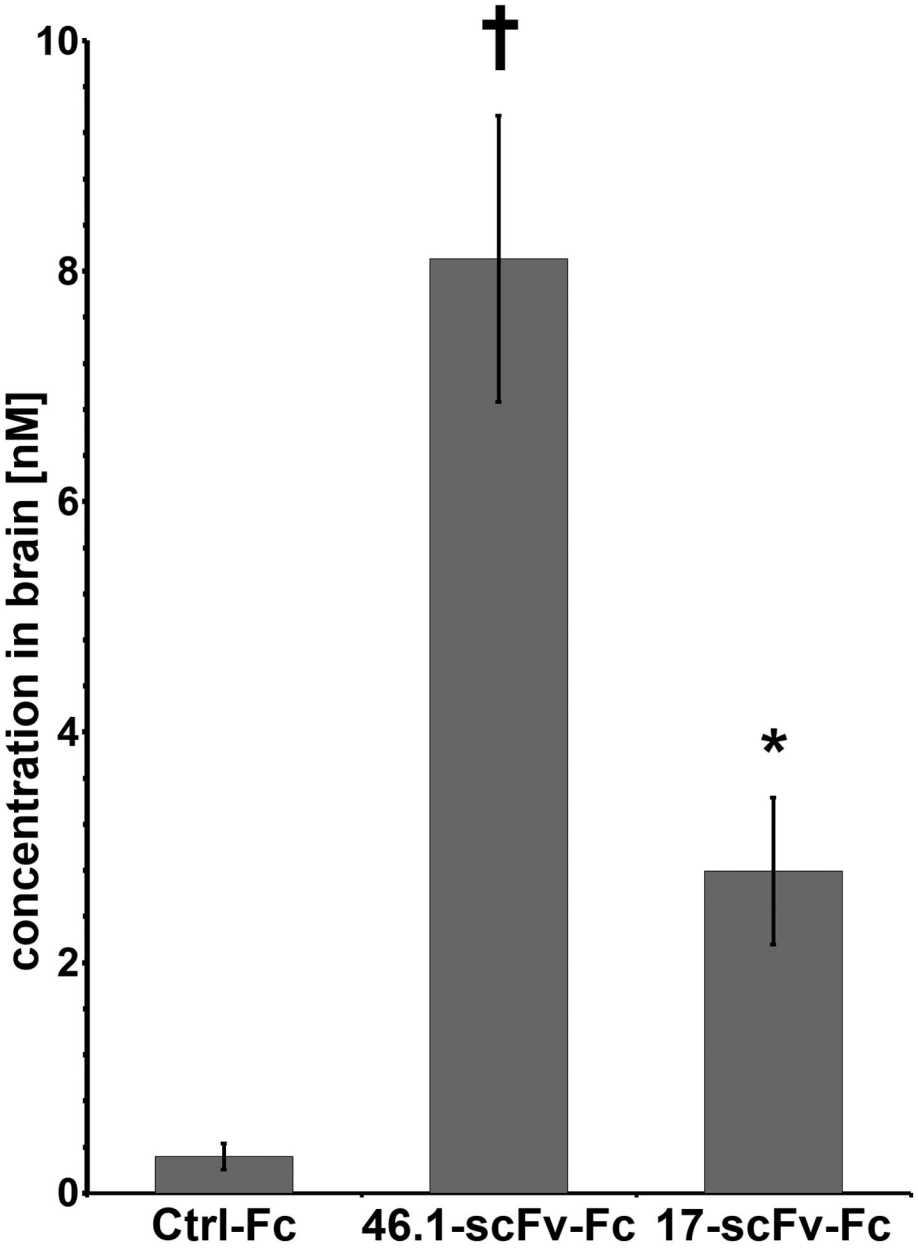

Figure 5.

Quantification of scFv-Fc brain accumulation. Clones 17 and 46.1 were intravenously injected into mice (n=4). After one hour, the mice were whole body perfused, brains collected and antibodies extracted. Concentration of antibodies in brain extracts were determined with ELISA as described in Materials and Methods. Reported are means ±S.E.M., † $p<0.005$, * $p<0.05$ compared to Ctrl-Fc by two-tailed unpaired Student's *t*-test.

Table 1.

Number of phage displaying an irrelevant anti-botulinum neurotoxin scFv that were recovered in the basolateral, brain side chamber in the Transwell system as a function of transendothelial electrical resistance (TEER).

TEER ($ohm\text{-}cm^2$)	Total CFU Brain side
140	4.9×10^7
168	1.12×10^6
403	5.4×10^3
712	1.24×10^3
1302	812
1905	205

Table 2.

Antibody attributes. (ND – Not Determined)

Clone	Binding to BMECs	Internalization into BMECs	Binding to brain tissue		Target BBB after IV injection
			human	mouse	
3	Yes	Yes	Yes	Yes	Yes
9	Yes	Yes	Yes	Yes	No
17	Yes	Yes	Yes	Yes	Yes
26	Yes	Yes	Yes	Yes	Yes
46.1	Yes	Yes	Yes	Yes	Yes
22Ch	Yes	Yes	Yes	No	No
6i	Yes	No	No	ND	ND
5A	Yes	Yes	No	ND	ND
2F-scFv	Yes	Yes	Yes	Yes	ND
4B-scFv	Yes	Yes	Yes	Yes	ND
5E-0.4	Yes	No	Yes	Yes	ND
B3-R3	Yes	No	Yes	Yes	ND

Table 3.

Apparent equilibrium binding affinity of selected clones. The table shows numeric values for the best-fit equilibrium binding affinity (K_D) and associated 95% CI.

Clone ID	Kd [nM]	95% CI
3	52	(30, 74)
9	44	(27, 60)
17	28	(19, 36)
26	38	(29, 47)
46.1	153	(128, 179)

Table 4.

Antibody organ biodistribution summary. (+ positive, − negative, ND not determined)

Clone	Brain	Heart	Lung	Liver	Kidney	Spinal cord
3-scFv-Fc	+	+	+	+	+	+
9-scFv-Fc	−	−	−	+	−	+
17-scFv-Fc	+	+	+	+	+	+
26-scFv-Fc	+	−	−	+	−	ND
46.1-scFv-Fc	+	−	+	+	+	+
Ctrl-Fc	−	−	−	−	−	−

Table 5.

Brain to plasma ratios were calculated from terminal plasma concentration of antibodies.

Clone	Brain concentration	Plasma concentration	Brain to plasma ratio
Ctrl-Fc	0.31 ± 0.11 [nM]	1970 ± 130 [nM]	0.015 ± 0.004 (%)
46.1-scFv-Fc	8.1 † ± 1.2 [nM]	1150 ± 100 [nM]	0.72 † ± 0.152 (%)
17-scFv-Fc	2.79 * ± 0.63 [nM]	940 ± 90 [nM]	0.28 † ± 0.045 (%)

Reported are means ±S.E.M.,

* p<0.05,

† p<0.005 compared to Ctrl-Fc by two-tailed unpaired Students *t*-test.